

Photodisintegration studies on p-nuclei: The case of Mo and Sm isotopes

C Nair†, A R Junghans†, M Erhard†, D Bemmerer†, R Beyer†, P Crespo†, E Grosse†‡, M Fauth†, K Kosev†, G Rusev†, K D Schilling†, R Schwengner†, and A Wagner†

† Institut für Strahlenphysik, Forschungszentrum Dresden-Rossendorf, Postfach 510119, 01314 Dresden, Germany

‡ Institut für Kern- und Teilchenphysik, Technische Universität Dresden, 01062 Dresden, Germany

E-mail: chithra.nair@fzd.de

Abstract. In explosive stellar environments like supernovae, the temperatures are high enough for the production of heavy neutron-deficient nuclei, the so-called p-nuclei. Up to now, the knowledge of the reaction rates of p-nuclei is based on theoretical parameterizations using statistical model calculations. At the bremsstrahlung facility of the superconducting electron accelerator ELBE of FZ Dresden-Rossendorf, we aim to measure the photodisintegration rates of heavy nuclei experimentally. Photoactivation measurements on the astrophysically relevant p-nuclei ^{92}Mo and ^{144}Sm have been performed with bremsstrahlung end-point energies from 10.0 to 16.5 MeV. First experiments on the short-lived decays following the reaction $^{144}\text{Sm}(\gamma, n)$ are carried out using a pneumatic delivery system for rapid transport of activated samples. The activation yields are compared with calculations using cross sections from recent Hauser-Feshbach models.

PACS numbers: 25.20.-x, 26.30.+k, 26.50.+x, 27.60.+j

Submitted to: *JPG*

1. Introduction

The nuclei heavier than iron ($Z > 26$) are synthesized mainly by neutron-capture reactions - the astrophysical r- and s- processes. The 35 neutron deficient stable isotopes between Se and Hg that are shielded from the rapid neutron capture by stable isobars are classically referred to as the p-nuclei. From the current understanding, best possible sites for the production of p-nuclei are O-Ne rich layers of Type II supernova explosions. Their production mechanism is understood as chains of photodisintegrations like (γ, n) , (γ, p) and (γ, α) on r- or s- seed nuclei [1, 2, 3]. The solar system isotopic abundances of the p-nuclei are generally only in the order (0.01-1)%. For an overview on the experimental techniques, status and problems associated with p-nuclei studies, see [4, 5].

For p-process nucleosynthesis modelling, precise knowledge of the astrophysical reaction rates is important. Despite the efforts in recent years, very few experimental

data for photodisintegration cross sections exist. Therefore, the reaction rates presently used are based on the cross sections obtained from Hauser-Feshbach statistical model calculations. The aim of our experiments with real photons is to determine the cross sections experimentally to test the statistical model calculations.

The present paper focuses on the results from photodisintegration studies of the *p*-nuclei ^{92}Mo and ^{144}Sm . The nuclide ^{144}Sm has been in the frame of the *p*-process chronometer ^{146}Sm [6]. There were several efforts to determine the $^{146}\text{Sm}/^{144}\text{Sm}$ production ratio experimentally which varies due to uncertainties in different inputs entering into the calculation, see [7]. One of the important nuclear physics input is the proper optical potential at energies of astrophysical relevance which has been derived from $^{144}\text{Sm}(\alpha,\alpha)^{144}\text{Sm}$ elastic scattering [8]. We have investigated the $^{144}\text{Sm}(\gamma,\alpha)^{140}\text{Nd}$ reaction via photoactivation method for the first time. With the rapid transport system for activated samples, the short-lived nuclides following the reaction $^{144}\text{Sm}(\gamma,n)^{143}\text{Sm}$ were identified. Photodisintegration studies on ^{92}Mo are performed aiming to test the underprediction of the Mo species in the network calculations. Preliminary results from ^{92}Mo data have been presented [10, 11].

2. Experimental Setup

In order to study the photodisintegration reactions on ^{92}Mo and ^{144}Sm , photoactivation measurements are being performed at the bremsstrahlung facility of the superconducting electron accelerator ELBE (Electron Linear accelerator of high Brilliance and low Emittance) of FZ Dresden-Rossendorf [12, 13]. ELBE delivers electron beams of energies up to 20 MeV with average currents up to 1 mA which is appropriate for probing photon-induced reactions.

The primary electron beam is focussed onto one of the several niobium radiators with thicknesses varying between 1.7 mg/cm² and 10 mg/cm² corresponding to $1.6 \cdot 10^{-4}$ and $1 \cdot 10^{-3}$ radiation lengths. Behind the radiator, the electron beam is separated from the photons by a dipole magnet and dumped into a graphite cylinder with a conical recess. The length of the cylinder is 600 mm and diameter is 200 mm. The photoactivation site is located behind the beam dump where available photon fluxes amount up to $10^9 \text{ cm}^{-2} \text{ s}^{-1} \text{ MeV}^{-1}$, see Station B in Fig. 1.

In this high-flux photoactivation area, targets of Mo or Sm were irradiated together with Au samples. At the same time another Au sample was irradiated together with a ^{11}B sample at the photon-scattering site, which is separated from the high-flux site by a heavy-concrete wall. A 2.6 m long collimator placed in the wall shapes the photon beam that hits the photon-scattering target with a photon flux of about $10^8 \text{ cm}^{-2} \text{ s}^{-1} \text{ MeV}^{-1}$. Photons scattered from ^{11}B were measured with four high-purity germanium (HPGe) detectors surrounded by escape-suppression shields consisting of bismuth-germanate (BGO) scintillation detectors. The photon flux at the photon-scattering site was determined by means of the known integrated cross sections of the states in ^{11}B depopulating via γ rays. Using the known cross section for the $^{197}\text{Au}(\gamma, n)$ reaction and the activities of the Au samples at the photon-scattering site and the high-flux site, the activation yields of the Mo and Sm isotopes were deduced.

The molybdenum targets used were of natural abundance (discs with mass 2-4 g and diameter 20 mm). For the activation of samarium we used fine Sm_2O_3 powder filled in polyethylene capsules (mass 3-4 g and diameter 18 mm). Au samples were of mass ≈ 200 mg and were irradiated both in the photoactivation site and in bremsstrahlung cave.

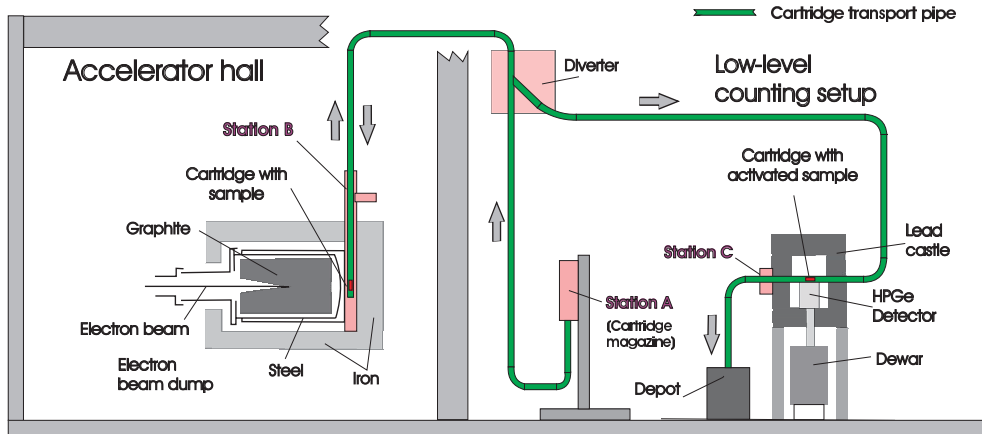


Figure 1. Pneumatic delivery system for fast transport of activated samples from irradiation site to the decay measurement site. The different stations for sample loading (A), irradiation (B) and decay measurement (C) is shown.

The number of activated nuclei produced during the activation was determined offline by measuring the decay in a low-level counting setup by HPGe with an efficiency 90% or 60% relative to a 3"×3" NaI detector.

3. The Rabbit System

An air-driven pneumatic delivery system (rabbit system) has been built for experiments with short-lived isotopes resulting from activation. A sketch of the setup is shown in Fig. 1. The whole system uses compressed air to transport the samples through polyamide (PA) tubes with a diverter making way to the to-and-fro movement of the sample cartridges. The samples to be irradiated are enclosed in polyethylene cassettes and loaded in Station A. They are shot to the high photon flux area behind the vacuum steel vessel aligned on the axis of the electron beam (Station B). After irradiation, the samples are transported within about 15 s to the lead-shielded low-level counting setup where the decay is measured with a coaxial HPGe detector. The loss time of 15 seconds arises from the time taken for transport of the sample plus placing the sample center above the HPGe detector. The variation in horizontal positioning of the samples by the rabbit system is very small, as the samples are stopped and then pushed back into position by a slowly operating pneumatic feedthrough. After the decay measurement, samples are shot to a radiation shielded container (depot, see figure).

The gamma-ray spectra for an activated sample of Samarium after 10 minutes of irradiation using the rabbit system is shown in Fig. 2. In the overlaid figure on the left panel, upper spectrum was taken 1 minute after an irradiation and the lower one after 9 minutes. The decays following $^{144}\text{Sm}(\gamma, n)^{143m}\text{Sm}$ and $^{144}\text{Sm}(\gamma, n)^{143}\text{Sm}$ reactions with half-lives 66 s and 8.75 min respectively are clearly seen. The $^{144}\text{Sm}(\gamma, n)^{143m}\text{Sm}$ reaction is identified with the unique line at 754 keV and the $^{144}\text{Sm}(\gamma, n)^{143}\text{Sm}$ with the lines above 1000 keV. On the right panel, exponential decay of the ground state of ^{143}Sm is shown. The measured half-life is 8.83 ± 0.08 min which

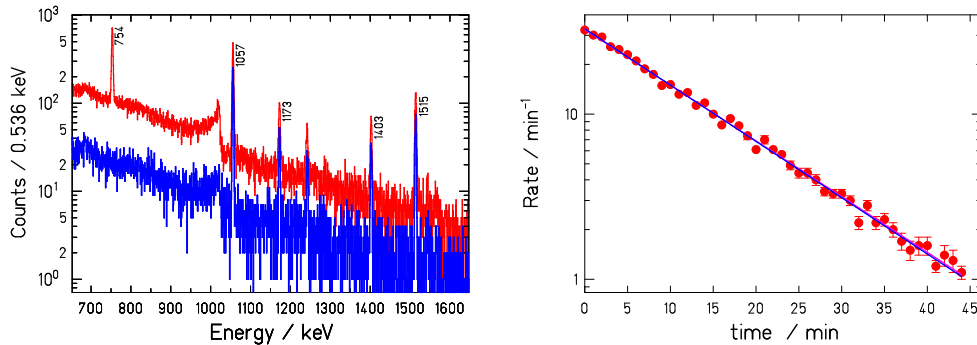


Figure 2. Decay spectra following the reaction $^{144}\text{Sm}(\gamma, n)$. The γ -ray energies are marked for the transitions from the decay of the isomeric and ground states of ^{143}Sm . On the right panel, exponential decrease in the rate of ^{143}Sm identified with the strongest line at 1057 keV is shown which was used for the half-life determination.

is in good agreement with the recent literature value 8.75 ± 0.08 min [14].

4. Data Analysis

In activation experiments, the sample to be studied (target) is irradiated always with a gold sample as normalization standard. The reaction $^{197}\text{Au}(\gamma, n)$ is well suited as a standard for activation experiments and has been measured previously by different methods [15, 16, 17]. The number of ^{196}Au nuclei produced during the activation is determined by counting the gamma decay in the shielded detector setup. The absolute efficiency of the HPGe detectors is based on measurements with several calibration sources from PTB and Amersham (systematic uncertainty in activity 0.6-1.5%) in the energy range from 0.12 to 1.9 MeV [18]. The sources were positioned at the same distance as the center of the irradiated samples. The effect of source extension and self-absorption of gamma-rays was determined with EFFTRAN [19] and GEANT3 [20] simulations. For the counting geometry directly on top of the detector the efficiency of the Sm_2O_3 samples is reduced by 3% compared to the point source value, whereas for the rabbit-system counting geometry the efficiency is reduced by 2%. Coincidence summing effects are minimized by using a Cd absorber with 1.5 mm thickness. They depend strongly on the decay scheme. The three dominant decay transitions of ^{196}Au used for analysis are at 333, 356 and 426 keV. For the transition at 333keV, the coincidence summing correction amounts to 24% and for 356 keV it is 6% both with a relative uncertainty of 5%.

The number of radioactive nuclei $N_{\text{act}}(E_0)$ produced in a photo-activation experiment is proportional to the integrated product of the absolute photon flux $\Phi_\gamma(E, E_0)$ and the photodisintegration cross section $\sigma_{\gamma, x}(E)$ with the integral limits from the reaction threshold energy E_{thr} up to the bremsstrahlung spectrum end-point energy E_0 . The symbol $x = n, p, \alpha$ denotes the emitted particle.

$$N_{\text{act}}(E_0) = N_{\text{tar}} \cdot \int_{E_{\text{thr}}}^{E_0} \sigma_{\gamma, x}(E) \cdot \Phi_\gamma(E, E_0) dE \quad (1)$$

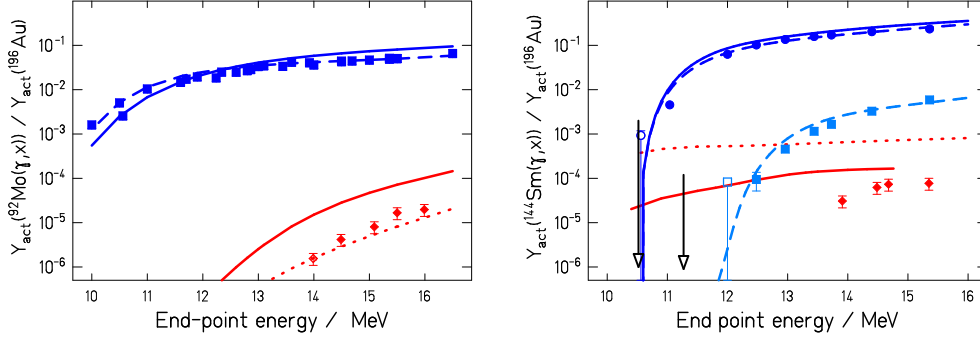


Figure 3. Experimental activation yields for photodisintegration reactions in ^{92}Mo (left) and ^{144}Sm (right) isotopes normalized to the $^{197}\text{Au}(\gamma,n)$ yield. For ^{92}Mo , the $^{92}\text{Mo}((\gamma,p)+(\gamma,n))$ (squares) and $^{92}\text{Mo}(\gamma,\alpha)$ (diamonds) yields are shown. On the right panel, the $^{144}\text{Sm}(\gamma,n)$ yields from ^{143}Sm (circles) and ^{143m}Sm (squares) decay are plotted together with the $^{144}\text{Sm}(\gamma,\alpha)$ yield (diamonds). The effective neutron separation energies for the respective $^{144}\text{Sm}(\gamma,n)$ reactions are marked by arrows and open symbols denote the detection threshold for the lowest measured energies. The dashed and dotted lines denote yield calculations using cross sections from TALYS [22] for the respective (γ,n) and (γ,α) reactions. The solid lines stand for predictions with cross sections from NON-SMOKER [21] code for both reactions.

After irradiation, the number of radioactive nuclei $N_{act}(E_0)$ is determined experimentally by measuring the decay using a HPGe detector and the formula reads:

$$N_{act}(E_0) = \varepsilon^{-1}(E_\gamma) \cdot N_\gamma(E_\gamma, E_0) \cdot p^{-1}(E_\gamma) \cdot \kappa_{corr} \quad (2)$$

$N_\gamma(E_\gamma, E_0)$, $\varepsilon(E_\gamma)$, $p(E_\gamma)$ stand for the dead-time and pile-up corrected full-energy peak counts of the observed transition, the absolute efficiency of the detector at the energy E_γ and the emission probability of the photon with energy E_γ respectively. The factor κ_{corr} accounts for the decay losses during irradiation, in between irradiation and decay measurements and during the measurement.

The activation yield is denoted by Y_{act} and is expressed as the ratio of the number of activated nuclei to the number of target atoms in the sample. For example, for the $^{92}\text{Mo}(\gamma,\alpha)$ reaction,

$$Y_{act} = N_{act}(^{92}\text{Mo}(\gamma,\alpha)) / N_{tar}(^{92}\text{Mo}) \quad (3)$$

The experimental data are compared to the yield integrals calculated with a simulated thick-target bremsstrahlung spectrum and photodisintegration cross sections predicted by Hauser-Feshbach models [21, 22].

5. Results and Discussion

Measured activation yields relative to the $^{197}\text{Au}(\gamma,n)$ reaction yield for photodisintegration reactions in ^{92}Mo and ^{144}Sm are shown in Fig. 3. In ^{144}Sm , the neutron separation energy is 10.5 MeV and the proton separation energy 6.7 MeV. The $^{144}\text{Sm}(\gamma,n)$ reaction produces ^{143}Sm or ^{143m}Sm . Since both of them are short-lived the irradiation was carried out using the rabbit system, see Sect. 3. The measured activation yield for $^{144}\text{Sm}(\gamma,n)^{143}\text{Sm}$ and $^{144}\text{Sm}(\gamma,n)^{143m}\text{Sm}$ reactions relative to the standard

$^{197}\text{Au}(\gamma, n)$ yield agrees within 20% to the simulated yield integrals with cross sections predicted by theoretical models [21, 22].

The $^{144}\text{Sm}(\gamma, \alpha)$ reaction was identified by the transition at 1596 keV from ^{140}Pr which is the short-lived daughter of the (γ, α) reaction product ^{140}Nd . For ^{144}Sm the $Q(\alpha)$ value is -0.145 MeV. Half-lives for ^{140}Nd and ^{140}Pr are 3.37 days and 3.4 minutes respectively. Measured reaction yields compared to the calculated ones are shown in Fig. 3. The preliminary experimental data for $^{144}\text{Sm}(\gamma, \alpha)$ relative yield is much below the simulated values. The theoretical models [21, 22] in this case differ strongly which could be an indication for the different α -nucleus potentials entering into the calculation. The predictions given by the two models are also dependent on the different parametrization of dipole strength functions, level densities and the mass models used. The experiment on $^{144}\text{Sm}(\gamma, p)$ reaction is in progress.

In ^{92}Mo , the experimental yields for $^{92}\text{Mo}((\gamma, p) + (\gamma, n))$ agree with the simulations using predicted cross sections from [21, 22] within 20%. For the (γ, α) , predictions from [22] agree within a factor of 2 whereas the one from [21] is much above the experimental value.

Acknowledgments

We thank the ELBE-team for providing the stable beam, J. Claussner and his co-workers for building the rabbit system and A. Hartmann for continuing technical assistance.

References

- [1] Woosley S E, Howard W M, *Astrophys. J. Suppl.* 36 (1978) 285.
- [2] Rayet M et al., *Astron. Astrophys.* 227 (1990). 271
- [3] Lambert D L, *Astron. Astrophys. Rev.* 3, 201 (1992).
- [4] Arnould M, Goriely S, *Phys. Rep.* 384 (2003) 1.
- [5] Mohr P et al., *Eur. Phys. J. A* 32, (2007) 357.
- [6] Audouze J, Schramm D N, *Nature* 237 (1972) 447.
- [7] Somorjai E et al., *Astron. Astrophys.* 333 (1998) 1112.
- [8] Mohr P et al., *Phys. Rev. C* 55 (1997) 1523.
- [9] Yin Q et al., *Nature* 415 (2002) 881.
- [10] Erhard M et al., *Eur. Phys. J. A* 27 s01 (2006) 135.
- [11] Erhard M et al., *PoS (NIC-IX)* 056 (2006).
- [12] Schwengner R et al., *Nucl. Instr. Meth A* 555 (2005) 211.
- [13] Wagner A et al., *J. Phys G: Nucl. Part Phys.* 31 (2005) S1969.
- [14] Evaluated Nuclear Structure Data File: <http://www.nndc.bnl.gov/ensdf>
- [15] Vogt K et al., *Nucl. Phys. A* 707 (2002) 241.
- [16] Veyssiere A et al., *Nucl. Phys. A* 159 (1970) 561.
- [17] Berman B L, et al., *Phys. Rev. C* 36 (1987) 1286.
- [18] Physikalisch Technische Bundesanstalt, Fachbereich 6.1, Bundesallee 100, Braunschweig, Germany; Amersham: ISOTRAK AEA Technology QSA, Gieselweg 1, Braunschweig, Germany.
- [19] Vidmar T et al., *Nucl. Instr. Meth A* 550 (2005) 603.
- [20] CERN program Library Long Writeup Q121, CERN, Geneva (CH), 1994
- [21] Rauscher T, Thielemann F -K, *At. Data Nucl. Data Tables* 88 (2004) 1.
- [22] Koning A J et al., *AIP. Conf. Proc.* 769 (2005) 1154.